Journal of Polymer Research (2024) 31:261
https://doi.org/10.1007/s10965-024-04109-x

ORIGINAL PAPER

Characterization of the interaction of nitric oxide/nitrogen dioxide with the polymer surfaces in ECMO devices

Moritz Köglmaier[1] · Thilo Joost[2] · Matthias Kronseder[3] · Werner Kunz[1]

Received: 17 May 2024 / Accepted: 12 August 2024

Abstract
In this work, the interactions between nitric oxide (NO)/nitrogen dioxide (NO_2) and the polymer materials of a gas exchanger system used in an extracorporeal membrane oxygenation (ECMO) setting are characterized. FTIR-ATR, XPS, and SEM were used to analyze the effects of the gas treatment. The polymer materials used in the gas exchanger system consisted of polymethylpentene (PMP) hollow fiber membranes, inlet/outlet caps made of methyl methacrylate acrylonitrile butadiene styrene (MABS), casting material consisting of polyurethane (PU), and the gas hoses made of polyvinyl chloride (PVC). Gas treatment with NO and NO_2 was conducted, with exposure times ranging from 30 min to 10 days. The gas concentrations range from 80 to 1000 ppm in the case of NO_2 and a maximum of 10,000 ppm in the case of NO. The formation of nitro and nitrate ester groups and nitric acid (HNO3) adsorption on the polymers' surface was observed using FTIR-ATR and XPS. The investigations showed that these effects depend on exposure time and gas concentration. The alterations persisted over more extended periods. The XPS measurements showed that the reaction only occurred exclusively on the surface of the polymers. The recorded SEM images showed no macroscopic changes in the surface structures of the polymers.

Keywords FTIR-ATR · XPS · SEM · ECMO · Hollow fiber membrane

Introduction

Theoretical background

Nitric oxide (NO) is a diatomic reactive molecule originally mainly known as an atmospheric pollutant released primarily due to fossil fuel burning [1, 2]. In the biological context, NO is produced by NO synthase and its cell-specific isoforms. The biological role of NO as a vasodilator was first discovered by F. Murad et al. in 1977 [3]. Subsequent discoveries were made by R. Furchgott et al. [4] in 1980 and L. Ignarro et al. [5] in 1987. Since then, a broad range of functionality has been elucidated. The biological function of NO, which is vital for this research, is its antithrombotic functionality. NO binds to the heme site of soluble guanylate cyclase (SGC), leading to the conversion of magnesium guanosine 5'-triphosphate to guanosine 3',5'-monophosphate (cGMP). cGMP then inhibits the phosphorylation of protein kinase C and decreases intracellular Ca^{2+} content, inhibiting platelet aggregation [6–9]. This antithrombotic functionality of NO is of particular importance for the self-regulation of platelets. The platelets release NO as they aggregate, limiting further aggregation [9, 10].

The second important gas in the context of this research is nitrogen dioxide (NO_2). Compared to NO, it is more reactive [11] and, therefore, more toxic. The discussion of NO_2 centers mostly on its role as an ambient air pollutant [12–14]. NO_2 initiates autoxidation reactions with the unsaturated fatty acids in pulmonary lipids, causing their destruction, subsequent membrane damage, and cell death, leading to decreased respiratory function [15]. In addition, it can also cause damage to amino acids [12]. NO_2 must be considered in this context, as NO rapidly reacts with oxygen to NO_2. Therefore, any gas mixture containing NO also contains a significant concentration of NO_2 if it is in contact with air [16–19].

✉ Moritz Köglmaier
moritz.koeglmaier@chemie.uni-regensburg.de

[1] Institute of Physical and Theoretical Chemistry, University of Regensburg, 93040 Regensburg, Germany

[2] Hemovent GmbH, 52076 Aachen, Germany

[3] Institute of Experimental and Applied Physics, University of Regensburg, 93040 Regensburg, Germany

Published online: 20 August 2024

Extracorporeal membrane oxygenation (ECMO) is a life support technique most commonly employed with patients suffering from acute respiratory distress syndrome, among other conditions. Blood is taken from the patient's venous circulation and, with a pump, circulated through a so-called gas exchanger. The CO_2 is exchanged with oxygen via hollow fiber membranes in the gas exchanger. The ventilation gas is pumped through the inside of the hollow fiber membranes while the blood passes around the outside of the membrane. The microporous structure of the outside wall of the hollow fiber membrane facilitates gas exchange. After passing through the gas exchanger, the oxygen-saturated blood returns to the patient [20–25]. A common issue in the application of ECMO devices, particularly over more extended treatment periods, is thrombus formation in the device, a common problem in blood-contacting medical devices. In most cases, heparin is employed to suppress these coagulation tendencies [26, 27]. The research done here was part of a larger project to investigate the viability of NO as an additive to the gas mixture of ECMO devices to suppress thrombus formation as an alternative to heparin.

Compatibility between the ECMO circuit and these gases must be ensured to achieve the goal of utilizing NO as part of the ventilation gas mixture. As previously discussed, NO and NO_2 are reactive molecules [1, 11]. Therefore, the research presented here aimed to investigate their influence on the materials used in the oxygenator and ensure that the treatment with either gas would not negatively affect the functional properties of the polymers.

So far, there is extensive work concerning the interaction of NO_2 with polymers specifically. The first steps were made by T. Ogihara et al. in the mid-1960s. This research focused on the reaction between polyethylene and the addition reaction to C–C double bonds [28, 29]. Throughout the 1960s and 70 s, H. Jellinek et al. conducted substantial research into the reactions of NO_2 with a variety of polymers, such as butyl rubber, polyethylene, polypropylene, polystyrene, and polyurethane, among others, expanding on the findings of T. Ohigara et al. According to this research, NO_2 can cause chain scission, crosslinking reactions, and the formation of nitro groups through addition reactions to double bonds in the polymer chain [30–35]. More recently, E. Davydov et al. looked into the interaction of NO_2 and polymers, focusing on the ion radical mechanism by which nitrogen-containing radicals are formed in polymers in contact with NO_2 [36, 37].

Structure of the gas exchanger

The gas exchanger consists of various components made from different polymer materials. The following paragraph provides a short visual and verbal overview of the function and location of the components making up the gas exchanger:

The hollow fiber membranes used in the gas exchanger are the central part of the ECMO device. They are integrated into the gas exchanger in dense layers (see Fig. 1i). The layers are arranged in an alternating pattern, with each successive layer changing the fiber orientation by 90°. This membrane consists of polymethylpentene (PMP). The bulk of the PMP material is microporous, providing gas transfer capabilities. A thin diffusion layer of PMP sits on the outside of the hollow fiber membrane to avoid fluid ingress. The ends of the hollow fiber membranes are encased in polyurethane (PU), which acts as the main structural component of the gas exchanger (see Fig. 1g).

The inlet and outlet plate form the gas exchanger's top and bottom (see Fig. 1c,f). Both consist of methyl methacrylate acrylonitrile butadiene styrene (MABS) plastic and act as structural components for the main body of the gas exchanger. Integrated into both caps is a connector for the blood hoses. The so-called gas caps are clipped to the sides of the gas exchanger (see Fig. 1d). The gas caps, like the inlet and outlet plates, are made from MABS plastic. Two gas caps have integrated connectors for the gas hoses (see Fig. 1b). The gas caps with hose connectors are sealed to the body of the gas exchanger with silicone seals (see Fig. 1h). In comparison, the other two gas caps have no seals

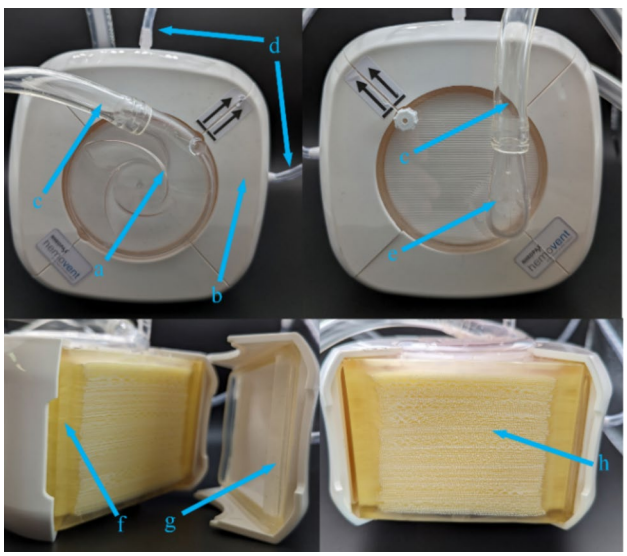

Fig. 1 Overview of the construction of the gas exchanger: (**a**) Blood hose (PVC) connected to the (**c**) inlet cap (MABS). (**b**) The gas hose (PVC) connected to the (**d**) gas cap (MABS). (**e**) Blood hose (PVC) connected to the (**f**) outlet cap (MABS). (**g**) PU-Material composing the main body of the gas exchanger. (**h**) Silicone gasket sealing the (**d**) gas cap (MABS) to the gas exchanger body. (**i**) The hollow fiber membrane (PMP) ends encased in the (**g**) PU-Material. The hollow fiber membranes (PMP) are visible behind the (**c**) inlet and the (**f**) outlet cap

to allow the remaining respiration gas to escape. Attached to the inlet/outlet cap and the gas caps are hoses made from polyvinylchloride (PVC) for blood and gas transport (see Fig. 1a,e). Of the two different PVC hoses, the gas hoses are used in this research.

The research presented here encompasses the treatment of PMP, MABS, PU, and PVC plastic surfaces with a variety of NO and NO_2 concentrations ranging from 80 to 10,000 ppm. PMP, MABS, and PU were chosen because they are all in direct contact with the patient's blood when the gas exchanger is in use. The gas hose (PVC) was selected due to its extended contact time with the gas mixture. The effects of the gas treatment were analyzed through Fourier transform infrared attenuated total reflection spectroscopy (FTIR-ATR), x-ray photoelectron spectroscopy (XPS), and scanning electron microscopy (SEM).

Results and discussion

FTIR-ATR results of the gas treatment

The initial FTIR-ATR spectroscopy experiments were conducted using a NO concentration of 10,000 ppm. The results of these initial measurements are shown below (see Figs. 2, 3, 4 and 5).

Visible in the spectra were mainly the signals caused by the polymers themselves. Starting at high wavenumbers, PU displayed a relatively broad signal at around 3330 cm^{-1}, corresponding to the N–H bond stretching vibration of the urethane groups (see Fig. S1c)[38]. All materials showed strong signals at just below 3000 cm^{-1} corresponding to the C-H-bond stretching vibrations of the carbon chains of the respective polymers [38]. The PU, MABS, and PVC spectra show strong carbonyl signals between 1730 and 1700 cm^{-1} (see Figs. S1b-d). For PU, that signal was caused by the carbonyl group contained in the urethane groups. For MABS, it was caused by the carbonyl group present in the methyl methacrylate monomer [38]. In contrast, the carbonyl signal in the spectra for the PVC hose was not caused by the polymer itself but by the ester groups of the plasticizer.

At around 1600 cm^{-1}, MABS and the PU showed signals corresponding to the quadrant stretching mode of the benzene rings of the styrene and methylene diphenyl diisocyanate (MDI) monomers, respectively. PU also displayed a signal at 1596 cm^{-1} corresponding to a C-N–H bending vibration (see Fig. S1c) [38]. Between 1500 and 1300 cm^{-1}, all materials showed signals corresponding to C-H bending vibrations and, in the case of PU, aromatic C = C stretching vibrations (see Fig. S1) [38]. At 610 cm^{-1}, the characteristic signal for the C–Cl stretching vibration of PVC was visible in the spectra (see Fig. S1d). Treating these materials with the NO-gas resulted in various additional signals. Some of them were visible in the regular spectra, such as the universally appearing signals at around 3400 and 1630 cm^{-1} (see Figs. 2b,c-5b,c).

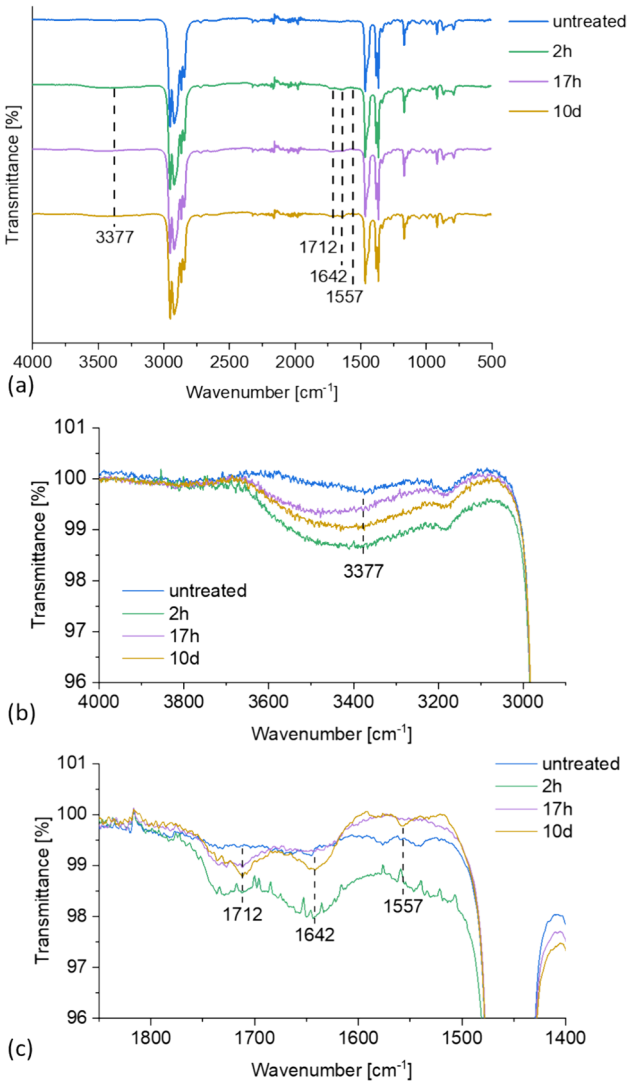

Fig. 2 FTIR-ATR spectra of PMP untreated and treated with NO (10,000 ppm) for two and 17 h, as well as ten days. (**a**) Overview of the spectra. (**b**) The signal at 3377 cm^{-1} caused by gas treatment. (**c**) Signals at 1712, 1642, and 1557 cm^{-1} caused by gas treatment. The marked signals were chosen based on the spectrum of the sample treated for ten days

Beyond that point, however, the dense array of signals the materials produced on their own in the region below 1600 cm^{-1}, combined with the relatively low signal height of the signals caused by the gas treatment, made further interpretation difficult. Therefore, additional measurements were performed using untreated samples of the respective material as the background to increase the visibility of the signals caused by the gas treatment (see Fig. 6). Using the untreated materials in the background measurements resulted in much better visibility of the signals caused by the gas treatment,

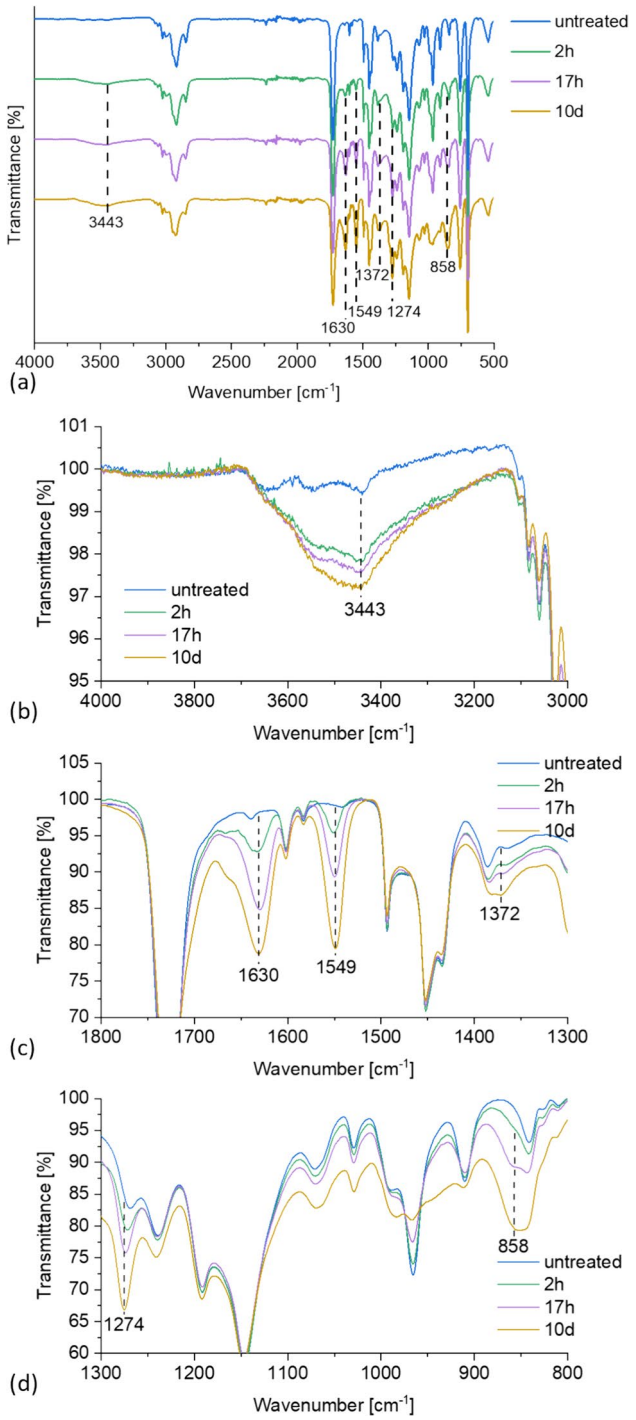

Fig. 3 FTIR-ATR spectra of MABS untreated and treated with NO (10,000 ppm) for two and 17 h, as well as ten days. (**a**) Overview of the spectra. (**b**) The signal at 3443 cm^{-1} caused by gas treatment. (**c**) Signals at 1630, 1549, and 1372 cm^{-1} caused by gas treatment. (**d**) Signals at 1274 and 858 cm^{-1} caused by gas treatment

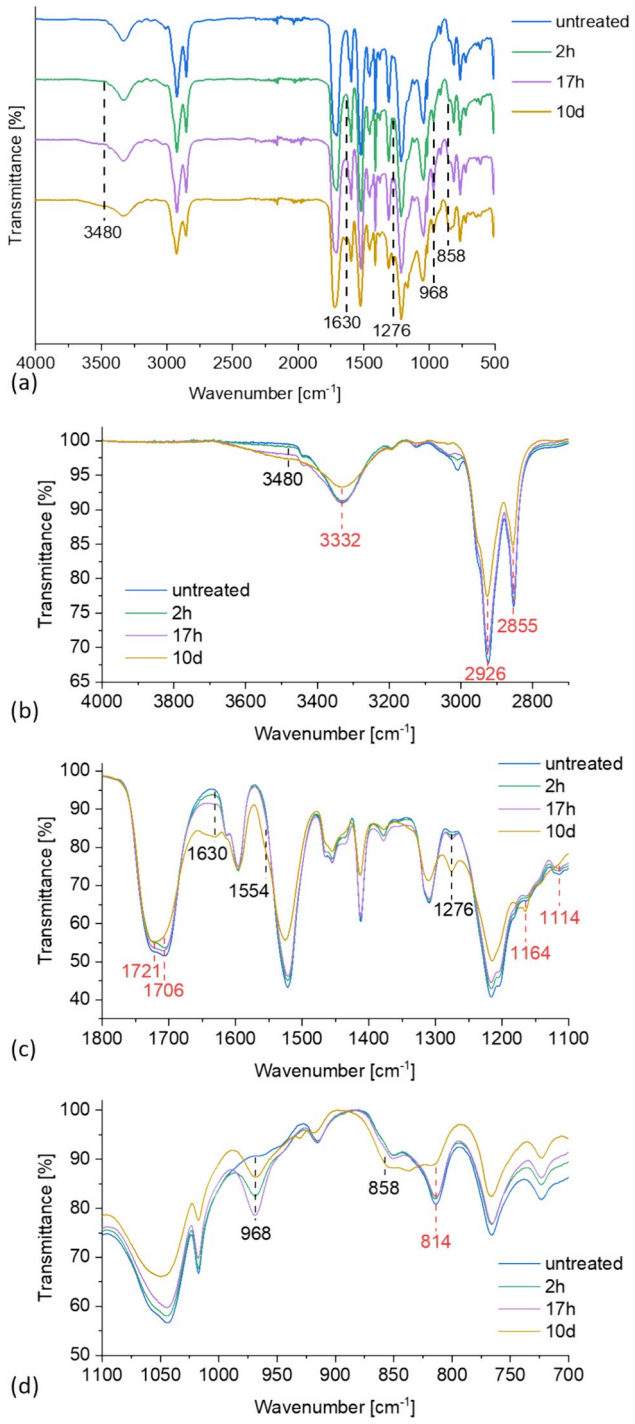

Fig. 4 FTIR-ATR spectra of PU untreated and treated with NO (10,000 ppm) for two and 17 h, as well as ten days. (**a**) Overview of the spectra. (**b**) The signal at 3480 cm^{-1} caused by gas treatment. (**c**) Signals at 1630 and 1276 cm^{-1} caused by gas treatment. (**d**) Signals at 968 and 858 cm^{-1} caused by gas treatment. Marked in red are the signals connected to cross-linking and chain scission reactions. The most significant of those signals are located at 3332, 2926, 2855, 1721, 1706, 1164, 1114, and 814 $cm.^{-1}$

especially in the fingerprint region. It is important to note that the difference spectra were not used to determine signal intensities or to identify new signals. They were merely used

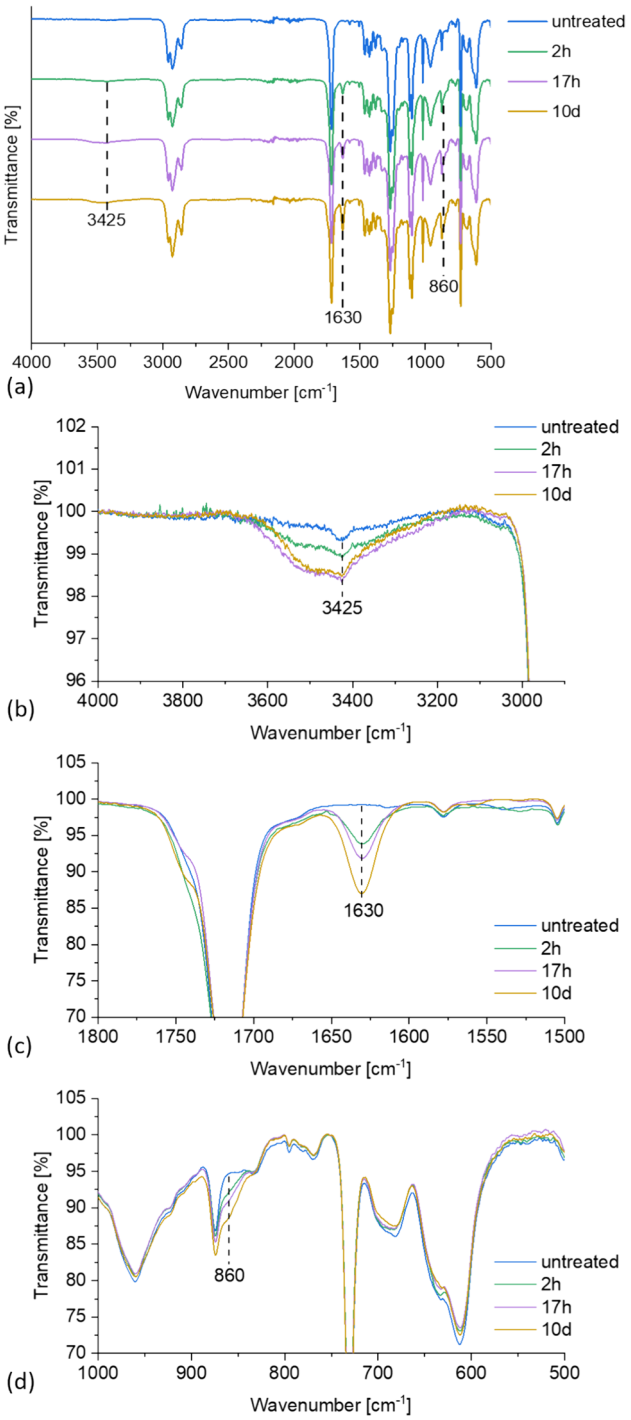

Fig. 5 FTIR-ATR spectra of PVC, untreated and treated with NO (10,000 ppm) for two and 17 h and ten days. (**a**) Overview of the spectra. (**b**) The signal at 3425 cm^{-1} caused by gas treatment. (**c**) Signal at 1630 cm^{-1} caused by gas treatment. (**d**) Signal at 860 cm^{-1} caused by gas treatment

to separate signals already visible in the regular spectra. No additional signals were identified.

Two signals were visible for all different materials. These include the broad signal between 3700 and 3200 cm^{-1} and the sharp signal at 1630 cm^{-1}. PMP alone displayed a signal at 1712 cm^{-1}. PMP, MABS, and PU also showed a signal between 1549 and 1557 cm^{-1} (see Fig. 6a-c). The PMP samples displayed no further signals below 1557 cm^{-1} (see Fig. 6 a). The other materials showed signals around 1276/1274 and 860/858 cm^{-1} (see Fig. 6b-d). In addition, PU displayed a signal at 968 cm^{-1} (see Fig. 6c), whereas MABS had an additional signal at 1372 cm^{-1} (see Fig. 6b).

The following functional groups and respective vibration modes were assigned to the signals originating from the NO treatment: The broad signal at around 3400 cm^{-1} and the signal at 1712 cm^{-1} likely stemmed from the adsorption of nitric acid (HNO_3) on the material's surface. The signal at 1712 cm^{-1} was only visible for PMP (see Fig. 6a), as the strong carbonyl signals of the other materials most likely overlayed this signal (see Fig. 6b-d). HNO_3 was formed via two subsequent reactions. In the first reaction, NO reacted with oxygen to NO_2:

$$2\ NO + O_2 \rightarrow 2\ NO_2 \quad (1)$$

NO_2 then reacted with water present in the air to HNO_3 [39]:

$$4\ NO_2 + 2\ H_2O + O_2 \rightarrow 4\ HNO_3 \quad (2)$$

As the gas mixtures in the gas bottles used for the experiments were dry, the formation of HNO_3 raises questions. Depending on the gas concentration used in the experiment, two different ways of HNO_3 formation are possible: At higher gas concentrations such as 10,000 and 1000 ppm, where just the gas bottle was used for the gas treatment, HNO_3 likely formed, as the gas was displacing the air in the treatment chamber. At these concentrations, NO reacts rapidly with oxygen to NO_2 [16]. This means that despite a dry gas mixture, a sizable concentration of NO_2 could have reacted with the moisture in the air before it was displaced. At a lower concentration of 80 ppm of NO, the bottled gas was mixed with compressed air produced by an Aquaforte Hi-flow V60 air pump (Sibo Fluidra Netherlands b.V., Doornhoek, Netherlands). The compressed air was produced from the surrounding air, so the NO_2 gas in the gas mixture was able to react with the moisture in the air throughout the entire gas treatment.

The signals at 1630, 1276/1274, and 860/858 cm^{-1} resulted from the formation of nitrate ester groups at the polymer surfaces. The 1630 and 1276/1274 cm^{-1} signals corresponded to the nitrate ester group's in-phase and out-of-phase stretching vibrations, while the 860/858 cm^{-1} signal corresponded to the NO stretching vibration of the

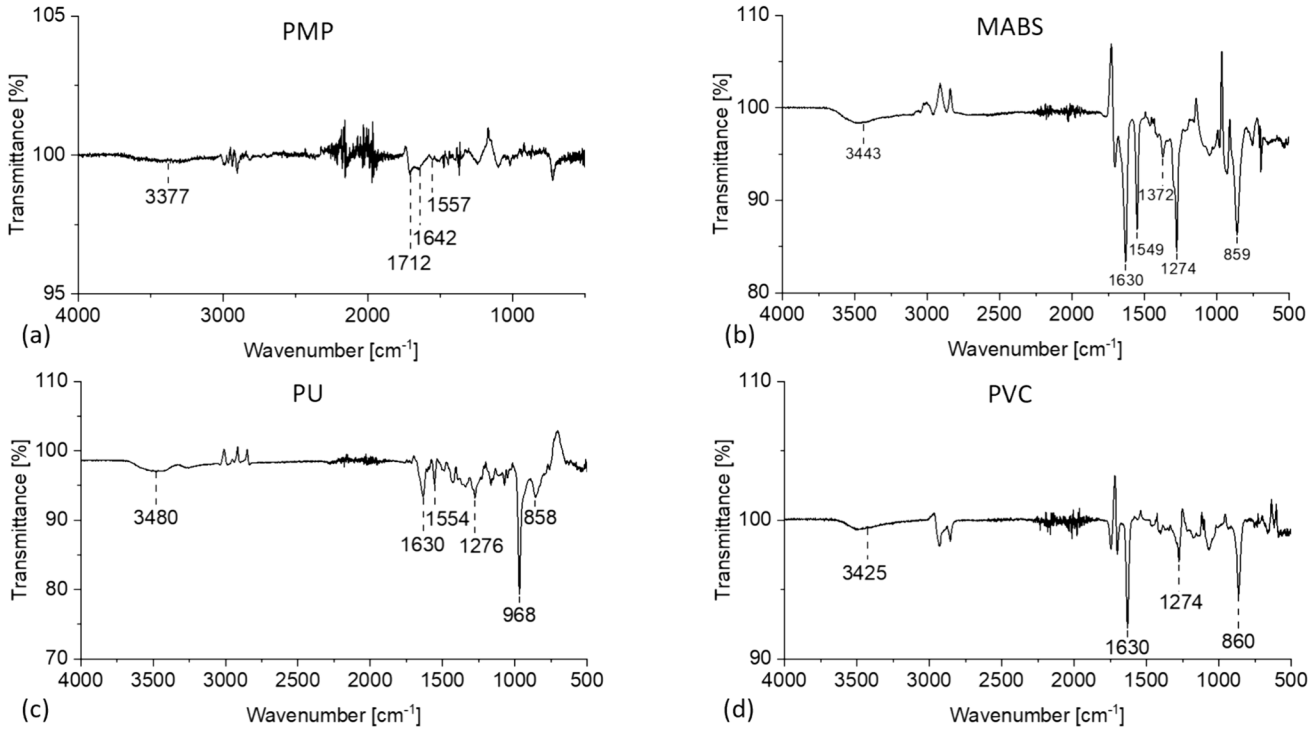

Fig. 6 FTIR-ATR difference spectra of (**a**) PMP, (**b**) MABS, (**c**) PU, and (**d**) PVC, treated with NO (10,000 ppm) for 17 h, using the respective untreated material as the background. The marked signals were identical to those observed in Fig. 3. For PU, the signal at 1554 cm^{-1} was additionally marked

group. The signals at 1549–1557 and 1372 cm^{-1} resulted from the formation of nitro groups. In this context, the signal at 1549–1557 cm^{-1} corresponded to the out-of-phase stretching vibration, and the signal at 1372 cm^{-1} to the in-phase stretching vibration of NO_2 [38]. The absence of both these signals in the spectra of PVC indicated that exclusively nitrate ester groups formed during the gas treatment. PU only displayed the signal at 1554 cm^{-1}, with the signal at 1372 cm^{-1} likely overlaid by existing PU signals. PU also showed a relatively strong signal at 968 cm^{-1} (see Fig. 6c), likely connected to HNO_3 adsorption [38].

Variations in the precise location of the signals between the different materials were observable. The range between 3377 and 3480 cm^{-1} in the case of the HNO_3 signal was the largest among them (see Figs. 2b-5b), with other signals having smaller ranges, such as the NO_2-signal ranging from 1549 to 1557 cm^{-1} for different polymers. These positional variations were due to the functional groups' different structural and chemical environments and deposited molecules [38].

Based on existing academic research, possible mechanisms for the formation of both the nitro- and nitrate ester groups can be formulated for the individual polymer materials. The most straightforward mechanism for the formation of nitro groups would have been the electrophilic addition of NO_2 to carbon–carbon double bonds, forming nitro and nitrite ester groups in a 3:1 ratio (see Scheme S1) [28, 40]. Possible attack points would have been the double bonds of the polybutadiene chain present in the MABS plastic (see Fig. S2). PMP, on the other hand, does not possess any carbon–carbon double bonds (see Fig. S2). This means that the addition reactions with NO_2 could have only proceeded at terminal monomers of the polymer chains or with residual monomers, which led to lower overall signal intensities (see Figs. 2a and 6a). In addition to the reactions with NO_2, HNO_3 could have also caused reactions leading to the formation of nitro groups. HNO_3 could have reacted in an electrophilic aromatic nitration reaction with the aromatic compounds of the polymers. This reaction occurs in a continuum between a polar and a single electron transfer (SET) mechanism. In both cases, the reaction proceeds through a π-complex followed by a transition state in the case of the polar mechanism and a SET intimate pair in the case of the SET mechanism. A σ-complex follows in both cases, with the abstraction of a proton as the final step (see Scheme S2) [41–43]. Potential reaction locations would have been the aromatic ring of the terephthalate-based ester DOTP used as a plasticizer in PVC. Other possible locations would have been the phenyl groups present in MABS and the benzene rings in the MDI-based diisocyanate monomer of PU (see Fig. S2). The fact that the PVC samples showed no signs of nitro group formation despite the presence of an aromatic

ring in DOTP was likely due to that ring being too sterically hindered to react with HNO_3 (see Fig. S2).

NO_2 could have also caused chain scission and crosslinking reactions in PU, as described by Pariiskii et al. and Jellinek et al. [11, 44]. In these mechanisms, NO_2 attacks the carbamate groups of the PU chain. It abstracts protons at the nitrogen atom of the carbamate group, the side chain of the tertiary amide groups, or the carbon atom directly neighboring the nitrogen atom in the polymer chain. Further reactions of these radicals could have led to either chain scission crosslinking reactions between radicals or nitration reactions with NO_2, leading to nitro and nitrite ester group formation (see Scheme S3) [11]. The only material that showed any signs of either crosslinking or chain scission reaction occurring was PU. The FTIR-ATR spectra measured after the treatment with NO (10,000 ppm) showed changes at 3332, 2926, 2855, 1721, 1706, 1164, 1114, and 814 cm^{-1} (see Fig. 4b-d). The decrease in signal intensity at 3332 cm^{-1}, the change in relative intensity between the signals at 1721 and 1706 cm^{-1}, and the appearance of the signal at 1164 cm^{-1} were all indicators for the occurrence of crosslinking reactions [45–47]. The decrease in signal height at 2926, 2855, 1114, and 814 cm^{-1}, as well as a decrease in signal height in the fingerprint region in general, on the other hand, indicated chain scission reactions [48–50]. None of the other polymers showed signs of cross-linking or chain scission reactions (see Figs. 2, 3, and 5). Based on existing research, the cross-linking and chain scission reactions should only be minor side reactions compared to the addition reactions with NO_2 [33, 34]. The chain scissions reactions observed at this concentration could be a potential concern for the mechanical stability of PU if they persisted at lower NO concentrations and occurred in the bulk of the polymer. The potential impact of chain scission reactions was further explored based on the XPS and SEM measurements. The chain scission and cross-linking reactions also had the potential to lead to the formation of nitro groups through a nitration side reaction between the radicals formed in the initial reaction step (see Scheme S3) and NO_2 [11]. However, the side reaction character of the chain scission and cross-linking reactions made it unlikely that this nitration reaction substantially contributed to the nitro groups' overall surface concentration.

Like with the nitro groups, several possible pathways exist to form nitrate ester groups on the polymer surfaces. The most straightforward mechanism would have been a secondary reaction to the addition reaction of NO_2 (see Scheme S1), where the unstable nitrite ester groups are converted into nitrate esters (see Scheme S4) [28, 51]. This mechanism would also explain the absence of signals in the spectra corresponding to the nitrite ester group. A second possible mechanism would have been the HNO_3 reaction with hydroxy groups. In the first step, HNO_3 reacted with itself to form both nitrooxonium and nitrate ions. A nitronium ion was then formed from the nitrooxonium ion in a second step. The nitronium ion then bonded to the oxygen atom of the hydroxy group, and the nitrate ion abstracted the proton from the oxygen, completing the formation of the nitrate ester group (see Scheme S5) [52, 53]. Possible attack points for this reaction would be unreacted hydroxy groups located in the PU material's polyol monomers. A variant of this mechanism involving an acid-catalyzed acid hydrolysis step is the likely explanation for the formation of nitrate ester groups in the PVC samples. Here, the ester groups of the plasticizer were hydrolyzed, catalyzed by HNO_3, with the formed hydroxy groups reacting with the HNO_3 molecules to form nitrate ester groups (see Fig. S2 and Schemes S5 and S6) [54]. The carboxyl groups resulting from the ester hydrolysis likely also played a role in forming the signal at 3425 cm^{-1} in addition to the HNO_3 molecules deposited on the surface (see Fig. 5a). Another possible location for this reaction would have been the methylmethacrylate monomers of MABS (see Fig. S2). Like the formation of nitro groups, the lack of functional groups ofthe PMP plastic led to very low corresponding signal strengths for this material (see Fig. S2).

The FTIR-ATR spectra were further analyzed in terms of the peak heights of selected signals. The signals at 3377, 1712, 1642, and 1557 cm^{-1} were chosen for PMP. For MABS, the signals at 3443, 1630, and 1549 cm^{-1} were analyzed. For PVC, the signals at 3425 and 1630 cm^{-1} were chosen. PU was not analyzed for peak heights as the signals caused by the gas treatment overlapped with the signals of the material itself. The difference spectra (see Fig. 6) were unsuitable for peak height analysis. The spectra were normalized based on the signal at 1466 cm^{-1} in the case of the PMP, the signal at around 1720 cm^{-1} in the case of MABS, and the signal at about 2927 cm^{-1} in the case of PVC.

For PMP, peak heights were overall low, with little visible progression in peak height over the treatment duration (see Fig. 7a). Gas treatment of MABS and the PVC resulted in a steep initial increase in signal strength (see Fig. 7b,c). Extending the treatment period to 10 days resulted in stronger signals, with a clear tendency towards saturation.

Further experiments were conducted, successively lowering the concentration of NO first to 1000 ppm and then to 80 ppm, to determine the dependence of the signal strength on gas concentration. The final application concentration of NO was planned at below 100 ppm.

Both 1000 and 80 ppm of NO resulted in lower signal intensities than the treatment with 10,000 ppm (see Figs. S3 and S4). The reaction of NO with oxygen to NO_2 was significantly slower at these concentrations, leading to much lower NO_2 concentrations and, subsequently, lower HNO_3 concentrations [16]. The spectra for PMP samples showed no additional signals after gas treatment (see Figs. S3a and

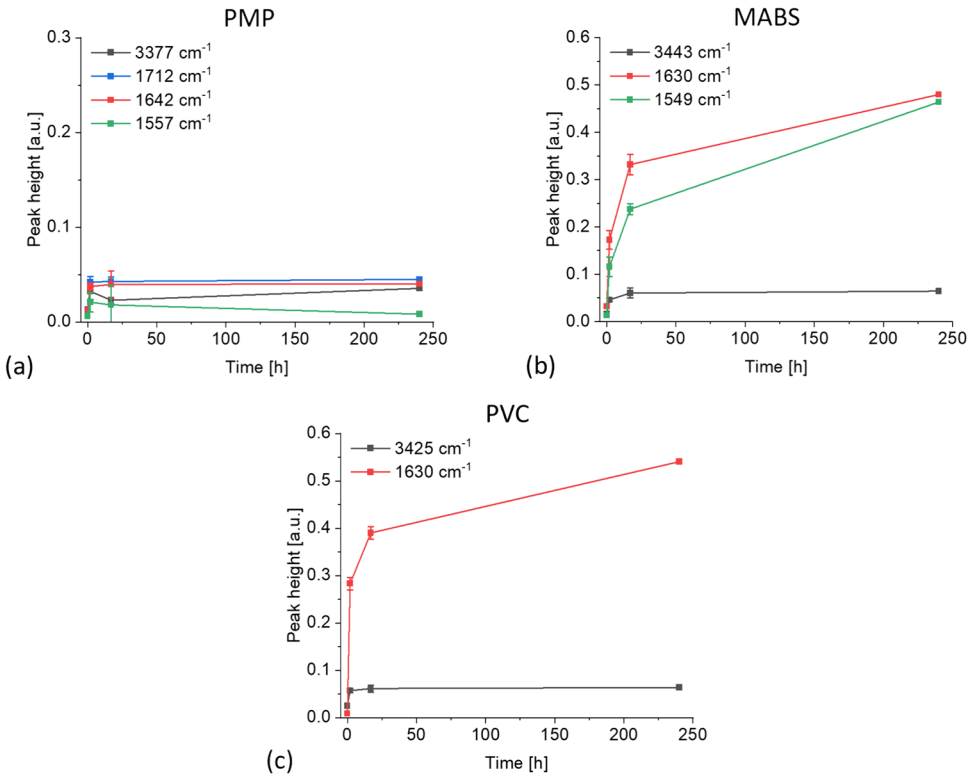

Fig. 7 Time evolution of the peak heights of the signals at 3377/3443/3425 cm^{-1} (black), 1712 cm^{-1} (blue), 1642/1630 cm^{-1} (red), and 1557/1549 cm^{-1} (green) of (**a**) PMP, (**b**) MABS, and (**c**) PVC during the treatment with NO (10,000 ppm). PMP generally showed low signal heights. MABS and PVC displayed a rapid increase in signal strength up to 17 h of gas treatment, which leveled off after that point

S4a). The signal strength was already very low compared to the other materials at 10,000 ppm NO (see Figs. 2–6). This meant that the gas treatment at lower concentrations resulted in signals below the detection limit. The signals appearing in the spectra were identical to those at the higher concentration for the remaining materials (see Fig. S3, S4, and S9). No indication for cross-linking or chain scission reactions of PU could be observed at either 1000 or 80 ppm. All the signals that showed a decrease when treated with 10,000 ppm remained unaffected at lower gas concentrations for treatment times up to 17 h (see Figs. S5 and S7). Extending the treatment time to 10 days, similar to the experiments with 10,000 ppm, resulted in only a slight decrease of the signals at 1721 and 1706 cm^{-1} at 1000 ppm and no changes connected with cross-linking or chain scission reactions at 80 ppm (see Figs. S6 and S8). This indicated that cross-linking and chain scission reactions were unlikely to be a concern at the actual application concentrations below 100 ppm.

The peak heights were analyzed identically to the gas treatment with 10,000 ppm NO (see Fig. 7). The spectra for the PMP samples were neglected in this case, as the signals resulting from the gas treatment were negligible in intensity. Due to the lower concentrations of NO and the shorter exposure time to the treatment gas, no saturation of the polymer surfaces was observed (see Figs. S10 and S11). The peak heights increased mostly linearly with increasing treatment time. At 1000 ppm, the values reached for the signal at 1557 cm^{-1} after 17 h of gas treatment were similar to those reached after the same treatment time with 10,000 ppm (see Figs. 7b and S10a) with a peak height of around 0.2. This value only decreased significantly at 80 ppm, reaching approximately 0.1 (see Fig. S11a). The peak height at 1630 cm^{-1} for MABS decreased from around 0.33 at 10,000 ppm to about 0.2 at 1000 and 80 ppm after 17 h (see Figs. 7b, S10a, and S11a). For PVC, the same signal did not decrease significantly (see Figs. 7c, S10b, and S11b), staying at around 0.2, independent of gas concentration. The peak heights for the signal at 3443 cm^{-1} decreased when going from 10,000 ppm to 1000 ppm of NO (see Figs. 7b,c, and S10). However, moving to a gas concentration of 80 ppm led to slightly higher peak heights than 1000 ppm (see Figs. S10 and S11). Overall, the drop in peak heights was not as pronounced as the drop in concentration from 10,000 to 80 ppm would indicate. However, these findings have to be qualified because the peak heights were much lower overall than the other analyzed signals, so even minor variations in peak heights could lead to an inconsistent relationship with the gas concentration.

So far, the theory was that NO_2, not NO, caused the reactions between the treatment gas and the polymer surfaces. Additional gas treatment experiments were conducted using NO_2 (1000 ppm) gas to confirm this assumption. Replacing NO with NO_2 resulted in very similar behavior of the polymer materials. Again, no additional signals could be observed for PMP (see Fig. S12a), identical to the treatment with NO (1000 ppm) (see Fig. S3a). For the remaining

materials, the additional signals were identical to the gas treatment with NO (see Figs. S12b,c,d, and S13). The spectra of PU showed no signs of cross-linking or chain scission reactions (see Fig. S14).

The peak heights were analyzed identically to those of gas treatments with NO. The spectra for PMP were again neglected, as the signals resulting from the gas treatment were negligible in intensity. The peak height results were very similar to the treatment results overall, with NO (1000 ppm) (see Figs. S10 and S15), with the final height just above 0.2 after 17 h of gas treatment.

Overall, the position of the signals caused by the gas treatment and the resulting peak heights indicate that NO was not responsible for the reaction with the polymer materials. Instead, NO_2 and HNO_3 were the reactive compounds.

Temporal stability of the gas treatment

In addition to the development of the peak heights during the gas treatment (see Figs. 7, S10, S11, and S15), the development of the peak heights after the end of the gas treatment was also analyzed. Samples treated with NO (1000 ppm) (see Fig. 8) and NO_2 (1000 ppm) (see Fig. S16) for 17 h were analyzed. The peak heights were normalized using the 1720 and 2927 cm^{-1} signals for MABS and PVC, respectively. PMP and PU were not analyzed. For PMP, the signal strengths at these gas concentrations were too low to be meaningfully analyzed. With PU, the overlap of the signals resulting from the gas treatment and the material made a peak height analysis impossible.

For MABS, the signals at 1630 and 1549 cm^{-1} dropped slightly during the first 24 h (see Fig. 8a). The peak heights leveled off after that point. For PVC, the signal at 1630 cm^{-1} also dropped slightly during the first 24 h, leveling off afterward (see Fig. 8b). The signal at 3443/3425 cm^{-1} remained constant for PVC (see Fig. 8b). For MABS, it showed the overall most substantial drop relative to the starting height compared to all other signals, losing one-third of its height (see Fig. 8a).

Little change was visible after the 17-h treatment with NO_2 (1000 ppm). Compared to the measurement directly after the gas treatment, the peak heights of the signals at 1630 and 1549 cm^{-1} dropped slightly over time (see Fig. S16a,b). The signal at 3443/3425 cm^{-1} remained stagnant for both materials.

In addition to the long-term stability tests under dry conditions, tests with the samples in contact with water were conducted to investigate the behavior of the samples in a scenario more closely resembling the actual application conditions. The signals remained constant for PVC, analogous to the long-term stability measurement (see Fig. 9b). Looking at MABS, the signal at 1549 cm^{-1} remained constant after contact with water, while the signal at 1630 cm^{-1} showed a slight decrease in signal strength in line with the decline seen for the same signal within the first 24 h of the long-term stability tests (see Fig. 8a). The signal at 3443 cm^{-1} saw the most significant decline relative to the original signal height, losing more than half its height compared to the measurements directly after the gas treatment (see Fig. 9a). The overall drop in signal height was more pronounced than the overall height loss for the long-term stability measurements with either NO or NO_2 (see Fig. 8a and S16a). Therefore, the results for MABS in contact with water showed a clear differentiation between covalently bound functional groups and molecules adsorbed on the surface. The signals at 1630 and 1549 cm^{-1} were attributed to covalently bound nitrate

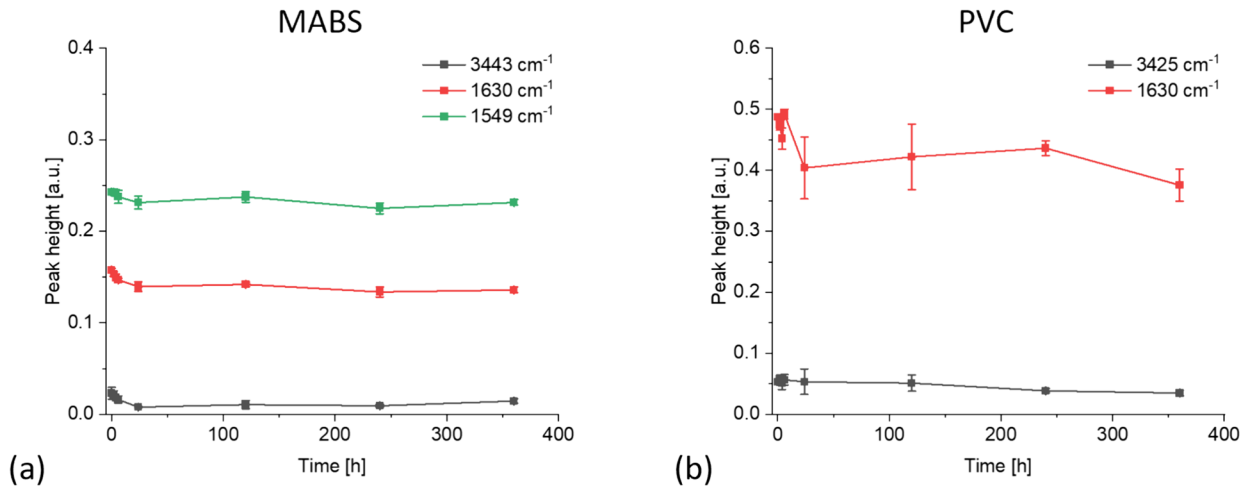

Fig. 8 The Time evolution of the peak heights of the signals at 3443 cm^{-1} (black), 1630 cm^{-1} (red), and 1557 cm^{-1} (green) of (**a**) MABS and (**b**) PVC after treatment with NO (1000 ppm) for 17 h. The signal strengths remained mostly constant after a slight initial decrease in the first 24 h

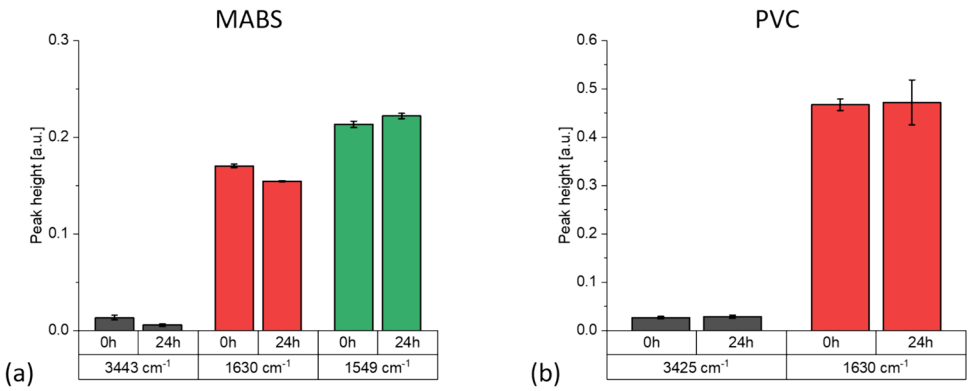

Fig. 9 Evolution of the peak heights of the signals at 3443/3425 cm^{-1} (black), 1630 cm^{-1} (red), and 1554 cm^{-1} (green) of (**a**) MABS and (**b**) PVC after treatment with NO (1000 ppm) for 17 h and immersion in water for 24 h. The signal strength behavior remained consistent with the long-term experiments under dry conditions, with only the MABS signal at 3443 cm^{-1} decreasing significantly more

ester and nitro groups. On the other hand, the signal at 3443 cm^{-1} was attributed to HNO_3 adsorbed on the surface of the samples. As these HNO_3 molecules were not bound to the polymers, the treatment with water resulted in most of the molecules being washed off, resulting in a decrease in height for the corresponding signal. For PVC, the adsorption of the HNO_3 molecules was likely stronger than for MABS, leading to a more stable signal independent of the treatment method (see Fig. 8b, S16b, and 9b).

XPS measurements

XPS measurements were conducted to verify the findings and interpretations of the FTIR signals caused by the gas treatment and to gain an understanding of the penetration depth of the interaction between NO and the polymers. The penetration depth of the interactions would be a strong indicator of whether the gas treatment affected the structural properties of the polymers or not. The samples were limited to PMP, MABS, and PU, as the PVC samples were unsuitable for XPS measurements due to their shape. Due to a constant energetic shift of all spectra by charging effects, all spectra were aligned to the normal C–C peak position of the C-1 s peak. The focus of the investigation was the nitrogen N-1 s peak in the binding energy range from 398 to 400 eV of both untreated and treated samples (see Figs. 10, 11, S17). The goal was to detect changes in the N-1 s peak position due to the formation of nitro and nitrate ester groups caused by the gas treatment. The spectra were fitted, and the visible peaks were deconvoluted using a Gauss peak function.

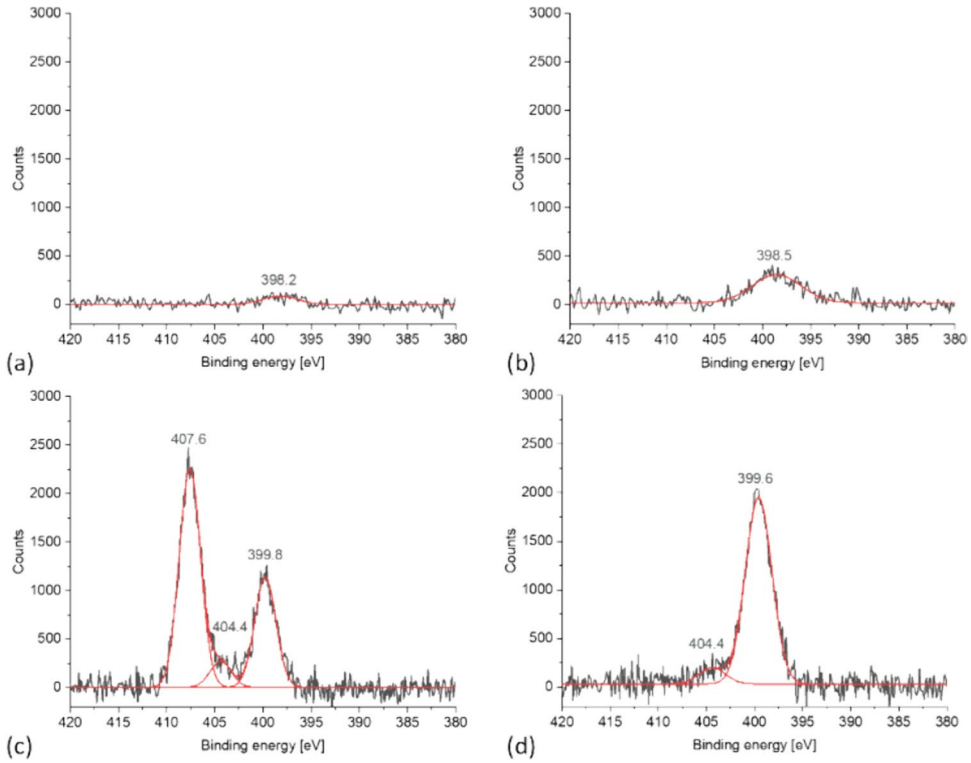

Fig. 10 XPS spectra of (**a**) untreated, (**b**) untreated and sputtered, (**c**) treated, and (**d**) treated and sputtered MABS samples. Gas treatment was conducted with NO (1000 ppm) for 17 h

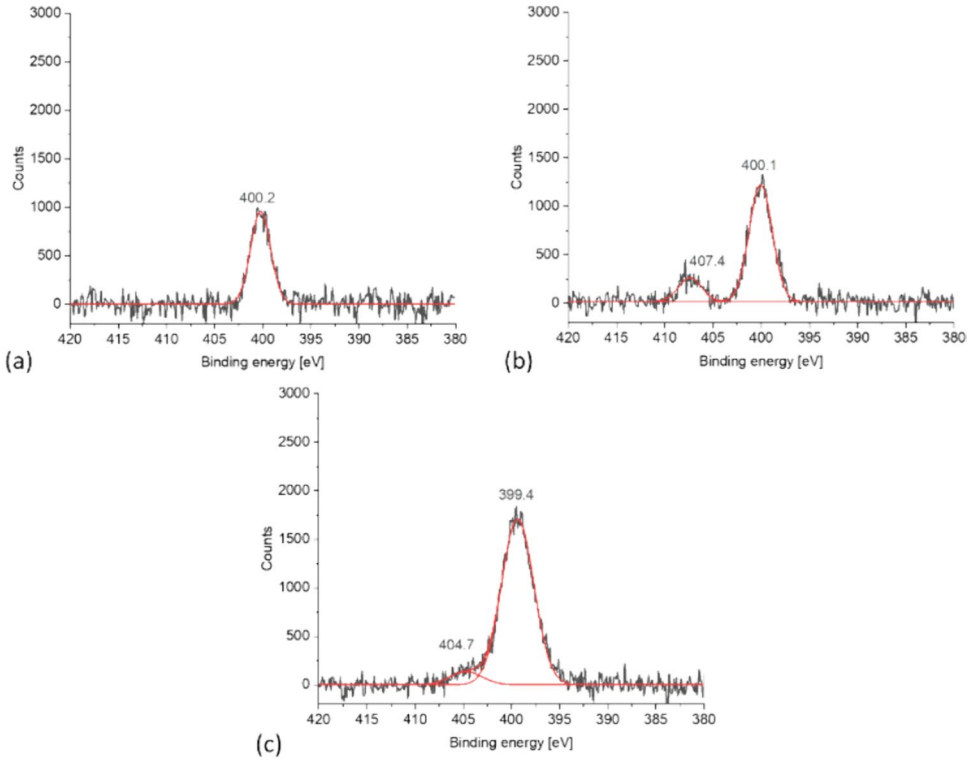

Fig. 11 XPS spectra of (**a**) untreated, (**b**) treated, and (**c**) treated and sputtered PU samples. Gas treatment was conducted with NO (1000 ppm) for 17 h

The spectra were analyzed between 420 and 380 eV, focusing exclusively on the nitrogen N-1 s peaks present in the spectra.

The PMP samples showed no changes due to the gas treatment, with the weak nitrogen peak remaining at 399.9 eV (see Fig. S17). Measurements with sputtered PMP samples were not possible due to unstable and long-term charging effects of the samples. These results align with the FTIR-ATR measurements, where no additional signals were found due to PMP lacking the structural features to react with either NO_2 or HNO_3 (see Fig. S2 and S3a). Gas treatment of MABS samples resulted in the nitrogen peak splitting into a total of three peaks (see Fig. 10). The original nitrogen peak located between 400 and 398 eV was likely caused by the nitrile group of the acrylonitrile monomers (see Fig. 10 a,b) [55]. Two additional peaks at 407.6 and 404.4 eV appeared after the gas treatment (see Fig. 10c). The peak at 407.6 eV was caused by the formation of nitrate ester groups and the adsorption of HNO_3 molecules [56, 57]. These results were confirmed by two additional samples used for stability measurements (see Fig. S18a,b). After sputtering the sample, the peak at 407.6 eV disappeared, leaving the peak at 399.6 eV and a small shoulder at 404.4 eV (see Fig. 10d).

The spectra of the PU samples again showed a nitrogen peak at around 400 eV caused, in this case, by the urethane groups of the polymer (see Fig. 11a) [58]. Measurements with the sputtered untreated samples were not possible due to excessive charging of the sample. Gas treatment resulted in the formation of a peak at 407.4 eV (see Fig. 11b). These results were confirmed by two additional samples used for stability measurements (see Fig. S19a,b). This peak was caused by the formation of nitrate ester groups and the adsorption of HNO_3 [56, 57]. Like MABS, this peak disappeared after the sputtering process, leaving behind the peak at 399.4 eV and a shoulder at 404.7 eV (see Fig. 11c).

In the case of MABS and PU, no peaks corresponding to nitro groups could be observed. This was likely due to limitations in the resolution of the spectra, with the peak expected at around 406 to 407 eV [56, 59]. The disappearance of the peaks corresponding to HNO_3 and nitrate ester groups proved that these functional groups were formed exclusively on the sample surface, as the peaks disappeared once the sputtering process had removed the topmost layer of material (see Figs. 10d, 11c). These results, therefore, strongly indicated that the gas treatment was unlikely to affect any changes in the structural properties of the polymers due to the shallow penetration depths of the interactions with NO. This result was of particular importance with regard to the potential cross-linking and chain scission reactions of PU. These reactions could have substantially impacted the mechanical stability of the PU material if they had propagated into the bulk material. The peaks at 404.4 and 404.7 eV appearing in the MABS and PU samples were within the fit error and, therefore, not attributable.

Stability measurements of the peaks caused by the gas treatment were conducted analogously to the FTIR-ATR

measurements. MABS and PU samples were treated with NO (1000 ppm) for 17 h, and XPS measurements were performed directly after the gas treatment and six and 13 days after the end of the gas treatment (see Figs. S18 and S19). The samples were left in contact with air at room temperature between measurements. Two samples of each material were analyzed. The peak area around 407.6 eV was used as the measure of stability. The peak area showed a high degree of stability for both materials. With MABS, the peak area decreased from 5727 to 4816 CPSeV, a drop of 16%. With PU, the peak area stayed completely stable (see Fig. S20). These results confirmed the findings of the FTIR-ATR measurements, which also showed high degrees of stability for the functional groups formed due to the NO treatment (see Figs. 8,9, and S16).

SEM recordings of the polymer surfaces

With the FTIR-ATR and XPS measurements, the focus was the characterization of the chemical changes to the polymer surfaces. SEM images were recorded to investigate whether these chemical changes led to macroscopic changes to the surface morphology of the polymers, which would influence the behavior of the polymers in contact with liquid [60]. This is important to the oxygenator's functionality, as these materials are in direct contact with blood throughout the device's actual application. Of particular interest were the hollow fiber membranes (PMP), as a change in polymer morphology could influence the porous structure of the fiber shell and, therefore, its gas permeability.

Visible in the SEM images of PMP was the microporous structure inside the hollow fiber membrane (see Fig. 12a,b). The outside of the membranes was covered in a smooth so-called diffusion layer of PMP (see Fig. 12c,d). The recorded images showed very clearly that the gas treatment with NO (1000 ppm) had no impact on the morphology of the polymer. The porous structure visible from the inside of the fibers remained unchanged, indicating no interference of the gas treatment with the functionality of the fibers. The outside of the membrane also remained unchanged. The visible gash on the outside of the treated fiber (see Fig. 12d) was most likely due to the handling of the fiber. Images recorded with samples treated with NO (80 ppm) similarly show no changes to the internal structure of the hollow fiber (see Fig. S21).

Of secondary importance were MABS and PU. Both these materials represented the major structural components of the gas exchanger. It was, therefore, important that these materials did not exhibit any significant changes to ensure structural integrity. The SEM images for MABS showed a relatively smooth surface (see Fig. S22). Again, like PMP, no changes in the surface morphology were observed. The surface remained smooth after the gas treatment (see Fig. S22b). The surface of the PU samples was much rougher than the surfaces of the other materials (see Fig. S23). The structure of the surface is explained by the manufacturing process, where the PU material was shaved down to the

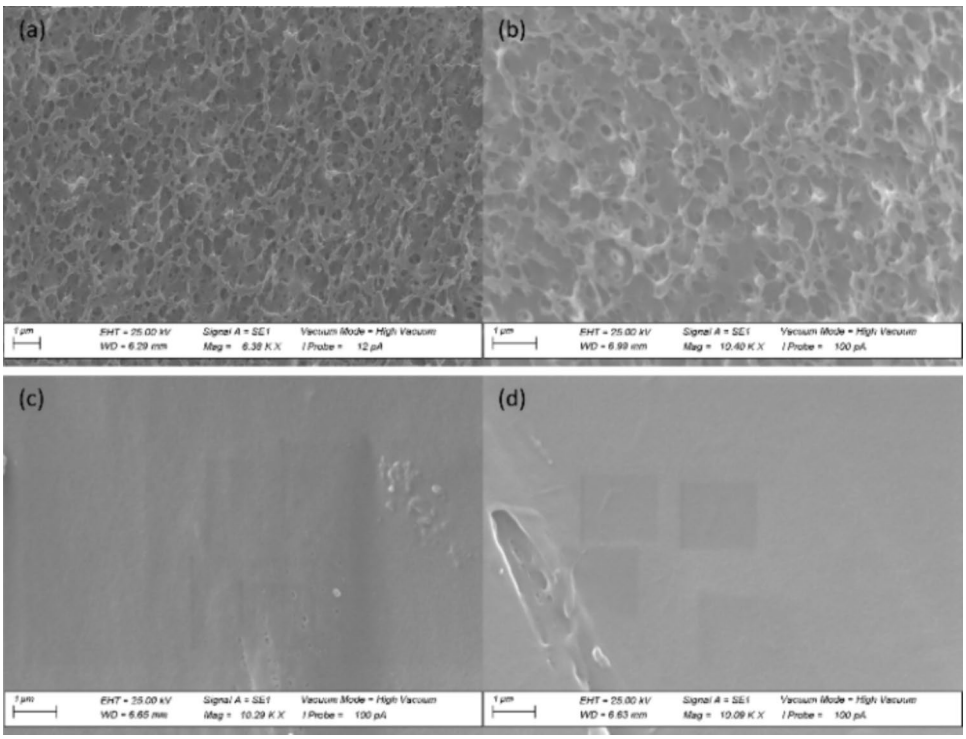

Fig. 12 SEM images of (**a**) the inside of an untreated hollow fiber membrane, (**b**) the inside of a hollow fiber membrane treated with 1000 ppm NO for 17 h hours, (**c**) the outside of an untreated hollow fiber membrane, and (**d**) the outside of a hollow fiber membrane treated with NO (1000 ppm) for 17 h at 6000 and 10.000 times magnification

correct size, resulting in the overall rough surface visible in the SEM images. In line with the results for both PMP and MABS, no change in surface morphology could be observed for PU. This result also indicated that no significant amount of cross-linking or chain scission reactions had taken place., as these reactions would have expressed themselves as visible changes in the surface of the polymer [47].

PVC was only of tertiary interest, as the gas hoses investigated here only represented an accessory to the ECMO circuit itself and are quickly replaceable should the need arise.

The untreated sample of PVC showed a smooth surface in the SEM images (see Fig. S24a). The treated sample showed no change in surface morphology caused by the gas treatment (see Fig. S24b). The partial hydrolysis of the plasticizer (see Scheme S6) had no visible impact on the surface morphology. The wrinkles that formed on the surface were likely due to the electron beam being focused on one part of the sample for too long, visible on the right edge of the image. The sample remained smooth on the undamaged left side of the image, indicating no significant changes happened due to the gas treatment.

The overall results of the SEM recordings showed that the gas treatment with NO (1000 ppm) caused no macroscopic changes to the surfaces of the polymers, strongly indicating that the utilization of NO in the would have no adverse effects on either the blood-contacting properties of the polymer surfaces or the gas permeability of the hollow fiber membranes.

Conclusions

Looking back at the goal set out in the introduction of this paper, the goal was to prove that the use of NO in the perfusion gas mixture did not negatively interfere with the functionality of the oxygenator. This paper showed that the treatment of polymer materials such as PMP, MABS, PVC, and PU with NO resulted in the formation of both nitro and nitrate ester groups through a variety of different mechanisms, as well as the adsorption of HNO_3 on the polymer surfaces, using both FTIR-ATR and XPS as analytical tools. The strength of these effects scaled with exposure time to the treatment gas but not necessarily with the gas concentration. Additionally, PU showed clear indications for cross-linking and chain scission reactions when treated with a NO concentration of 10,000 ppm. No such indications could be found at lower gas concentrations and with different analytical methods. The other polymers showed no indications of chain scission reactions occurring. The results of the XPS measurements proved that the functional groups formed because of the gas treatment were solely located at the surface of the polymer samples. The effects on the polymer materials were stable for a significant amount of time after the gas treatment under both dry and wet conditions, confirmed by both FTIR-ATR and XPS measurements. In the case of MABS, stability measurements in contact with water allowed for the differentiation between the covalently bound nitro and nitrate ester groups, which remained stable, and the HNO_3 molecules, which were largely washed away. It was also shown that NO was not responsible for the effects on the polymer surfaces, which were instead caused by NO_2 and HNO_3. The temporal stability of these functional groups meant that the newly formed functional groups were likely to remain stable under application conditions, limiting their potential transfer to the patient's bloodstream. While the effects of the gas treatment were visible at a relatively high concentration of 10,000 ppm used during this study, using concentrations of 1000 and 80 ppm resulted in weaker effects. Therefore, the impact on the polymer materials should have been minor at the final application concentration of 40 ppm or below. It was also significant that the hollow fiber membrane, the largest blood-contacting surface in the gas exchanger, showed no signs of gas treatment effects below 10,000 ppm. Therefore, functionality and hemocompatibility of the hollow fiber membrane should not be affected at application concentrations of NO. Chain scission and crosslinking reactions likely occurred to a certain degree, particularly with PU. However, based on existing research, they were likely minor side reactions compared to the addition reaction of NO_2 with C–C double bonds [33, 34]. XPS measurements confirmed these findings, also showing signals corresponding to HNO_3 molecules and nitrate ester groups. XPS also revealed that the influence of the gas treatment only extended to the very surface of the polymers, which strongly indicated that their structural properties should not be affected by the gas treatment. The SEM images showed no influence of the gas treatment, with none of the polymer samples displaying any macroscopic change in surface morphology. This was particularly of note for PMP, as it meant that the material retained its porous structure and, therefore, its gas transfer ability. At the same time, the results for MABS and PU meant that the surface morphology and, thus, the blood-contacting properties of the polymers should have remained unaffected. The use of NO in the perfusion gas mixture should not pose an issue for the functionality of the oxygenator based on the results gathered in this paper.

Experimental section

Chemicals and materials

NO (10,000 ppm in N_2), NO (1000 ppm in N_2), and NO_2 (1000 ppm in N_2) were purchased from basi Schöberl GmbH & Co. KG (Rastatt, Germany). Material samples of the gas

exchanger components, including hollow fiber membranes (PMP), inlet/outlet caps (MABS), gas hoses (PVC), and polyurethane sheets (PU), as well as fully assembled gas exchangers, were provided by Hemovent GmbH (Aachen, Germany). The hollow fiber membrane used was 3 M Membrana OXYPLUS, type PMP 90/200 (3 M Deutschland GmbH, Wuppertal, Germany). The PU sheets were made up of a prepolymer consisting of methylene diphenyl diisocyanate and glycols (Biresin DH41 Komp. B, Sika Deutschland GmbH, Stuttgart, Germany) and trimethylolpropane (Biresin DH404 Komp. A, Sika Deutschland GmbH, Stuttgart, Germany) (information provided directly by Sika Deutschland GmbH (Stuttgart, Germany). The MABS used was Terlux HD 2802, produced by INEOS Styrolution Group GmbH (Frankfurt am Main, Germany). The gas hoses were produced by Rehau SE (Bern, Switzerland) as Rauclair-E, containing the plasticizer bis(2-ethylhexyl) terephthalate (DOTP) (32.7 wt%) (information directly provided by Rehau SE (Bern, Switzerland)).

Gas treatment of the gas exchanger materials

The gas exchanger materials were treated with NO concentrations of 80, 1000, and 10,000 ppm. NO_2 was used at concentrations of 1000 ppm. The treatment durations most commonly investigated were 30 min, one hour, two hours, four hours, and 17 h. Treatment with 10,000 ppm of NO was performed for up to 10 days. Material samples were placed in a chamber for the treatment, and the gas mixture was added at a continuous flow rate of 2 L/min for up to four hours. The samples treated for 17 h hours were placed in the chamber, and the gas mixture was added. The chamber was closed during the inflow of treatment gas to keep the gas concentration constant. The hollow fiber membrane was treated by applying the gas mixture directly to a fully assembled gas exchanger. Small samples of hollow fiber membranes were taken from the gas exchanger at the corresponding time intervals.

To measure the temporal stability of the signals resulting from the gas treatment, treated samples were kept at room temperature and analyzed again using FTIR-ATR. Samples treated with 1000 ppm of NO and NO_2 were measured 2, 4, 6, 24 h, and five days after the gas treatment. The samples treated with NO additional measurements after 10 and 15 days were conducted.

In addition to the long-term stability measurements under dry conditions, short-term stability measurements with liquid contact were also conducted. For this purpose, samples were treated with NO (1000 ppm) and immersed in Millipore water for 24 h. Afterward, the samples were dried over silica gel in a desiccator for another 24 h. FTIR-ATR measurements were conducted directly after the gas treatment and after the drying process.

Gas treatments at concentrations of 1,000 and 10,000 ppm were conducted by directly attaching the respective gas bottles of NO and NO_2 in nitrogen to GT1355 Sho-Rate G rotameter (Brooks Instruments, Hatfield, PA, USA), which in turn was directly connected to the chamber. For the treatment with 80 ppm of NO, a NO-A nitric oxide delivery system (EKU Elektronik GmbH, Leiningen, Germany) was used in conjunction with an Aquaforte Hi-flow V60 air pump (Sibo Fluidra Netherlands b.V., Doornhoek, Netherlands). The flow rate was monitored with a SpiroScout EKU flowmeter (Ganshorn Medizin Electronic GmbH, Niederlauer, Germany).

Fourier transform infrared attenuated total reflection spectroscopy

FTIR-ATR measurements were conducted using an Agilent Varian 670 IR spectroscope (Agilent Technologies Inc., Santa Clara, CA, USA) with a Pike Technologies GladiATR probe head (Pike Technologies, Fitchburg, WI, USA). The spectra were recorded between 500 and 4000 cm^{-1} as the average of 16 scans with a resolution of 2 cm^{-1}. The samples (see Fig. 13) were pressed down onto the diamond of the ATR module to ensure complete coverage. It was possible to achieve consistent coverage of the diamond with reproducible signal intensities. Regular spectra (see Fig. 2–5) were recorded using a background measurement of the unoccupied sample space. Difference spectra (see Fig. 6) used a background measurement recorded with a sample of the respective untreated polymer placed on the diamond.

X-Ray photoelectron spectroscopy

XPS measurements were conducted using a Physical Electronics PHI 5700 (Physical Electronics GmbH, Feldkirchen, Germany). PMP, MABS, and PU samples were analyzed as untreated samples and samples treated with NO (1000 ppm) for 17 h. Each sample was measured both in its original and in a sputtered state. The sputtered samples were treated by Ar-ion-bombardment for ten minutes with a 1.9 kV acceleration voltage on a square area of 49 mm^2 in size, removing several nanometers of material. A neutralizer was used during both the measurement and

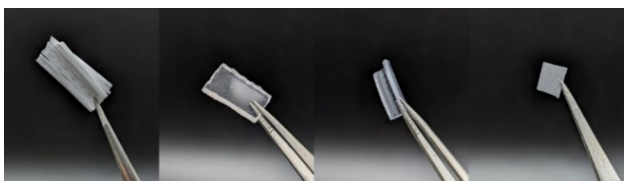

Fig. 13 From left to right: Samples of PMP, MABS, PVC, and PU used for FTIR-ATR measurements

the sputtering treatment to suppress the charging effects of the insulating samples.

Scanning *electron* microscopy

SEM recordings were taken of the gas exchanger materials samples before and after treatment with NO. The samples were sputter coated in gold using a Quorum SC 7620 sputter coater (Quorum Technologies, Lewes, United Kingdom) for 30 s. A Zeiss EVO MA15 scanning electron microscope (Carl Zeiss Ag., Oberkochen, Germany) with a backscattered electron detector was used to record the SEM images. For samples of the hollow fiber membrane, images of the inside and the outside of the fibers were recorded. For the remaining materials, the images were recorded on the side of the material in contact with the treatment gas in the fully assembled gas exchanger.

Supplementary Information The online version contains supplementary material available at https://doi.org/10.1007/s10965-024-04109-x.

Acknowledgements The authors would like to thank Mrs. Ulrike Schießl from the chair for inorganic chemistry of Professor Dr. Arno Pfitzner for conducting the REM measurements.

The authors would also like to thank Hemovent GmbH for the close cooperation and advice throughout the research project and for providing the experimental materials. Dr. Bernhard Hanke for his ideas and preliminary experiments forming the basis of this research. Dr. Rainer Köbrich for providing the NO-A device and his technical assistance throughout the project.

Author contributions Moritz Köglmaier: Formal analysis (lead), Investigation (lead), Methodology (equal), Data Curation (lead), Validation (lead), Visualization (lead), Writing – Original Draft (lead).

Matthias Kronseder: Formal analysis (equal), Investigation (equal), Methodology (equal), Data curation (equal).

Thilo Joost: Resources (lead), Conceptualization (equal), Project administration (equal).

Werner Kunz: Supervision (lead), Conceptualization (equal), Methodology (equal), Project administration (equal), Writing – Review & Editing (lead).

Data availability Data will be made available on request.

Declarations

Competing interests The authors declare that they have no known competing financial interests or personal relationships that could have influenced the work reported in this paper.

This research was supported by the ZIM program (Zentrales Innovationsprogramm Mittelstand or Central Innovation Program for small and medium-sized Enterprises (SME)) of the Federal Ministry for Economic Affairs and Climate Action under the research project "NOAMED – Stickstoffmonoxid zur Oberflächenmodifikation beim Einsatz von Gasaustauschern bei der extrakorporalen Lungenunterstützung " (KK 5023802AD0) conducted in cooperation with Hemovent GmbH (Aachen, Germany).

References

1. Carpenter AW, Schoenfisch MH (2012) Nitric oxide release: part II. Ther Appl Chem Soc Rev 41:3742–3752. https://doi.org/10.1039/c2cs15273h
2. Feldman PL, Griffith OW, Stuehr DJ (1993) The surprising life of NITRIC OXIDE. Chem Eng News 71:26–38. https://doi.org/10.1021/cen-v071n051.p026
3. Arnold WP, Mittal CK, Katsuki S et al (1977) Nitric oxide activates guanylate cyclase and increases guanosine 3':5'-cyclic monophosphate levels in various tissue preparations. Proc Natl Acad Sci USA 74:3203–3207. https://doi.org/10.1073/pnas.74.8.3203
4. Furchgott RF, Zawadzki JV (1980) The obligatory role of endothelial cells in the relaxation of arterial smooth muscle by acetylcholine. Nature 288:373–376. https://doi.org/10.1038/288373a0
5. Ignarro LJ, Buga GM, Wood KS et al (1987) Endothelium-derived relaxing factor produced and released from artery and vein is nitric oxide. Proc Natl Acad Sci USA 84:9265–9269. https://doi.org/10.1073/pnas.84.24.9265
6. Matsuoka I, Nakahata N, Nakanishi H (1989) Inhibitory effect of 8-bromo cyclic GMP on an extracellular Ca2+-dependent arachidonic acid liberation in collagen-stimulated rabbit platelets. Biochem Pharmacol 38:1841–1847. https://doi.org/10.1016/0006-2952(89)90420-6
7. Nakashima S, Tohmatsu T, Hattori H et al (1986) Inhibitory action of cyclic GMP on secretion, polyphosphoinositide hydrolysis and calcium mobilization in thrombin-stimulated human platelets. Biochem Biophys Res Commun 135:1099–1104. https://doi.org/10.1016/0006-291X(86)91041-7
8. Radomski MW, Moncada S (1993) Regulation of vascular homeostasis by nitric oxide. Thromb Haemost 70:36–41
9. Cheung PY, Salas E, Schulz R et al (1997) Nitric oxide and platelet function: implications for neonatology. Semin Perinatol 21:409–417. https://doi.org/10.1016/s0146-0005(97)80006-7
10. Kuo PC, Schroeder RA (1995) The emerging multifaceted roles of nitric oxide. Ann Surg 221:220–235. https://doi.org/10.1097/00000658-199503000-00003
11. Pariiskii GB, Gaponova IS, Davydov EY (2000) Reactions of nitrogen oxides with polymers. Russ Chem Rev 69:985–999. https://doi.org/10.1070/RC2000v069n11ABEH000611
12. Kikugawa K, Kato T, Okamoto Y (1994) Damage of amino acids and proteins induced by nitrogen dioxide, a free radical toxin, in air. Free Radic Biol Med 16:373–382. https://doi.org/10.1016/0891-5849(94)90039-6
13. Chen T-M, Gokhale J, Shofer S et al (2007) Outdoor air pollution: nitrogen dioxide, sulfur dioxide, and carbon monoxide health effects. Am J Med Sci 333:249–256. https://doi.org/10.1097/MAJ.0b013e31803b900f
14. Elsayed NM (1994) Toxicity of nitrogen dioxide: an introduction. Toxicology 89:161–174. https://doi.org/10.1016/0300-483X(94)90096-5
15. Pryor WA, Lightsey JW, Church DF (1982) Reaction of nitrogen dioxide with alkenes and polyunsaturated fatty acids: addition and hydrogen-abstraction mechanisms. J Am Chem Soc 104:6685–6692. https://doi.org/10.1021/ja00388a035
16. Skalska K, Miller J, Ledakowicz S (2010) Kinetics of nitric oxide oxidation. Chem Pap 64:269–272. https://doi.org/10.2478/s11696-009-0105-8
17. Wink DA, Ford PC (1995) Nitric oxide reactions important to biological systems: a survey of some kinetics investigations. Methods 7:14–20. https://doi.org/10.1006/meth.1995.1003
18. Tsukahara H, Ishida T, Mayumi M (1999) Gas-phase oxidation of nitric oxide: chemical kinetics and rate constant. Nitric Oxide 3:191–198. https://doi.org/10.1006/niox.1999.0232

19. Thomas DD (2015) Breathing new life into nitric oxide signaling: a brief overview of the interplay between oxygen and nitric oxide. Redox Biol 5:225–233. https://doi.org/10.1016/j.redox.2015.05.002
20. Allen S, Holena D, McCunn M et al (2011) A Review of the Fundamental principles and evidence base in the use of extracorporeal membrane oxygenation (ECMO) in critically Ill adult patients. J Intensive Care Med 26:13–26. https://doi.org/10.1177/0885066610384061
21. Cooper DS, Jacobs JP, Moore L et al (2007) Cardiac extracorporeal life support: state of the art in 2007. Cardiol Young 17(Suppl 2):104–115. https://doi.org/10.1017/S1047951107001217
22. Gattinoni L, Carlesso E, Langer T (2011) Clinical review: Extracorporeal membrane oxygenation. Crit Care 15:243–248. https://doi.org/10.1186/cc10490
23. Bartlett RH, Gattinoni L (2010) Current status of extracorporeal life support (ECMO) for cardiopulmonary failure. Minerva Anestesiol 76:534–540
24. MacLaren G, Combes A, Bartlett RH (2012) Contemporary extracorporeal membrane oxygenation for adult respiratory failure: life support in the new era. Intensive Care Med 38:210–220. https://doi.org/10.1007/s00134-011-2439-2
25. Makdisi G, Wang I-W (2015) Extra corporeal membrane oxygenation (ECMO) review of a lifesaving technology. J Thorac Dis 7:E166–E176. https://doi.org/10.3978/j.issn.2072-1439.2015.07.17
26. Jaffer IH, Fredenburgh JC, Hirsh J et al (2015) Medical device-induced thrombosis: what causes it and how can we prevent it? J Thromb Haemost 13(Suppl 1):S72-81. https://doi.org/10.1111/jth.12961
27. Gorbet MB, Sefton MV (2004) Biomaterial-associated thrombosis: roles of coagulation factors, complement, platelets and leukocytes. Biomaterials 25:5681–5703. https://doi.org/10.1016/j.biomaterials.2004.01.023
28. Ogihara T (1963) Oxidative degradation of polyethylene in nitrogen Dioxide. Bull Chem Soc Jpn 36:58–63. https://doi.org/10.1246/bcsj.36.58
29. Ogihara T, Tsuchiya S, Kuratani K (1965) Initial stage of the oxidation reaction of polyethylene by nitrogen dioxide. Bull Chem Soc Jpn 38:978–984. https://doi.org/10.1246/bcsj.38.978
30. Jellinek HHG, Toyoshima Y (1967) Reaction of nitrogen dioxide with polystyrene films. J Polym Sci A-1 Polym Chem 5:3214–3218. https://doi.org/10.1002/pol.1967.150051221
31. Jellinek HHG, Flajsman F, Kryman FJ (1969) Reaction of SO2 and NO2 with polymers. J Appl Polym Sci 13:107–116. https://doi.org/10.1002/app.1969.070130112
32. Jellinek HHG, Flajsman F (1969) Reaction of nitrogen dioxide with polystyrene films. J Polym Sci A-1 Polym Chem 7:1153–1168. https://doi.org/10.1002/pol.1969.150070412
33. Jellinek HHG, Flajsman F (1970) Chain scission of butyl rubber by nitrogen dioxide in absence and presence of air. J Polym Sci A-1 Polym Chem 8:711–726. https://doi.org/10.1002/pol.1970.150080314
34. Jellinek HHG (1973) Reactions of linear polymers with nitrogen dioxide and sulfur dioxide. Text Res J 43:557–560. https://doi.org/10.1177/004051757304301001
35. Jellinek HHG, Martin F, Wegener H (1974) Tensile strength of polyurethane exposed to nitrogen dioxide. J Appl Polym Sci 18:1773–1778. https://doi.org/10.1002/app.1974.070180615
36. Davydov EY, Gaponova IS, Pariiskii GB et al (2006) Ion-radical mechanism of polymer-nitrogen dioxide interaction. Polym Sci Ser A 48:375–381. https://doi.org/10.1134/S0965545X06040055
37 Davydov E, Gaponova I, Pariiskii G et al (2010) Reactivity of Polymers on Exposure to Nitrogen Dioxide. Chem Chem Technol 4:281–290. https://doi.org/10.23939/chcht04.04.281
38. Larkin P (2018) Infrared and Raman spectroscopy: Principles and spectral interpretation, 2nd edn. Elsevier, Amsterdam
39. England C, Corcoran WH (1974) Kinetics and mechanisms of the gas-phase reaction of water vapor and nitrogen dioxide. Ind Eng Chem Fund 13:373–384. https://doi.org/10.1021/i160052a014
40. Giamalva DH, Kenion GB, Church DF et al (1987) Rates and mechanisms of reactions of nitrogen dioxide with alkenes in solution. J Am Chem Soc 109:7059–7063. https://doi.org/10.1021/ja00257a025
41. Ridd JH (1971) Mechanism of aromatic nitration. Acc Chem Res 4:248–253. https://doi.org/10.1021/ar50043a003
42. de Queiroz JF, Carneiro JWdM, Sabino AA et al (2006) Electrophilic aromatic nitration: understanding its mechanism and substituent effects. J Org Chem 71:6192–6203. https://doi.org/10.1021/jo0609475
43. Kochi JK (1992) Inner-sphere electron transfer in organic chemistry. Relevance to electrophilic aromatic nitration. Acc Chem Res 25:39–47. https://doi.org/10.1021/ar00013a006
44. Jellinek HHG, Wang TJY (1973) Reaction of nitrogen dioxide with linear polyurethane. J Polym Sci Polym Chem Ed 11:3227–3242. https://doi.org/10.1002/pol.1973.170111216
45. Kontou E, Spathis G, Niaounakis M et al (1990) Physical and chemical cross-linking effects in polyurethane elastomers. Colloid & Polymer Sci 268:636–644. https://doi.org/10.1007/BF01410405
46. Tsai Y-M, Yu T-L, Tseng Y-H (1998) Physical properties of crosslinked polyurethane. Polym Int 47:445–450
47. Christenson EM, Anderson JM, Hiltner A (2007) Biodegradation mechanisms of polyurethane elastomers. Corros Eng Sci Techn 42:312–323. https://doi.org/10.1179/174327807X238909
48. Tcharkhtchi A, Farzaneh S, Abdallah-Elhirtsi S et al (2014) Thermal aging effect on mechanical properties of polyurethane. Int J Polym Anal Ch 19:571–584. https://doi.org/10.1080/1023666X.2014.932644
49. Wilhelm C, Gardette J-L (1998) Infrared analysis of the photochemical behaviour of segmented polyurethanes: aliphatic poly(ether-urethane)s. Polymer 39:5973–5980. https://doi.org/10.1016/S0032-3861(97)10065-9
50. Rosu D, Rosu L, Cascaval CN (2009) IR-change and yellowing of polyurethane as a result of UV irradiation. Polym Degrad Stab 94:591–596. https://doi.org/10.1016/j.polymdegradstab.2009.01.013
51. Gray P, Williams A (1959) The thermochemistry and reactivity of alkoxyl radicals. Chem Rev 59:239–328. https://doi.org/10.1021/cr50026a002
52. Boschan R, Merrow RT, van Dolah RW (1955) The chemistry of nitrate esters. Chem Rev 55:485–510. https://doi.org/10.1021/cr50003a001
53. Urbański T (1983) Chemistry and technology of explosives. Repr Pergamon Pr, Oxford
54. Shi H, Wang Y, Hua R (2015) Acid-catalyzed carboxylic acid esterification and ester hydrolysis mechanism: acylium ion as a sharing active intermediate via a spontaneous trimolecular reaction based on density functional theory calculation and supported by electrospray ionization-mass spectrometry. Phys Chem Chem Phys 17:30279–30291. https://doi.org/10.1039/C5CP02914G
55. Accolla M, Pellegrino G, Baratta GA et al (2018) Combined IR and XPS characterization of organic refractory residues obtained by ion irradiation of simple icy mixtures. A&A 620:A123. https://doi.org/10.1051/0004-6361/201834057
56. Beard BC (1990) Cellulose nitrate as a binding energy reference in N(1s) XPS studies of nitrogen-containing organic molecules. Appl Surf Sci 45:221–227. https://doi.org/10.1016/0169-4332(90)90005-K
57. Rouxhet PG, Doren A, Dewez JL et al (1993) Chemical composition and physico-chemical properties of polymer surfaces. Prog

Org Coat 22:327–344. https://doi.org/10.1016/0033-0655(93)80034-8
58. Sakagami Y, Horiguchi K, Narita Y et al (2013) Syntheses of a novel diol monomer and polyurethane elastomers containing phospholipid moieties. Polym J 45:1159–1166. https://doi.org/10.1038/pj.2013.48
59. Erkal A, Erdoğan MS, Aşık İ et al (2014) Electrografting and surface properties of some substituted nitrophenols on glassy carbon electrode and simultaneous Pb 2+ - Cd 2+ analysis via assist of graphene oxide terminated surface. J Electrochem Soc 161:H696–H704. https://doi.org/10.1149/2.1081410jes
60. Spori DM, Drobek T, Zürcher S et al (2008) Beyond the lotus effect: roughness influences on wetting over a wide surface-energy range. Langmuir 24:5411–5417. https://doi.org/10.1021/la800215r